

UC Irvine

UC Irvine Previously Published Works

Title

Methane oxidation in the eastern tropical North Pacific Ocean water column

Permalink

<https://escholarship.org/uc/item/5v72x8f4>

Journal

Journal of Geophysical Research G: Biogeosciences, 120(6)

ISSN

2169-8953

Authors

Pack, MA
Heintz, MB
Reeburgh, WS
[et al.](#)

Publication Date

2015

DOI

10.1002/2014JG002900

Peer reviewed

RESEARCH ARTICLE

10.1002/2014JG002900

Key Points:

- The first CH₄ oxidation (MO_x) rates in the eastern tropical Pacific (ETP) Ocean
- Water column MO_x strongly mitigates sea-air CH₄ flux in the ETP region
- Advances in rate measurements are needed to provide accurate ocean CH₄ budgets

Supporting Information:

- Supporting Information S1

Correspondence to:

M. A. Pack,
mpack@uci.edu

Citation:

Pack, M. A., M. B. Heintz, W. S. Reeburgh, S. E. Trumbore, D. L. Valentine, X. Xu, and E. R. M. Druffel (2015), Methane oxidation in the eastern tropical North Pacific Ocean water column, *J. Geophys. Res. Biogeosci.*, 120, 1078–1092, doi:10.1002/2014JG002900.

Received 31 DEC 2014

Accepted 7 MAY 2015

Accepted article online 14 MAY 2015

Published online 19 JUN 2015

Methane oxidation in the eastern tropical North Pacific Ocean water column

Mary A. Pack¹, Monica B. Heintz², William S. Reeburgh¹, Susan E. Trumbore¹, David L. Valentine², Xiaomei Xu¹, and Ellen R. M. Druffel¹

¹Department of Earth System Science, University of California, Irvine, California, USA, ²Department of Earth Science, University of California, Santa Barbara, California, USA

Abstract We report methane (CH₄) concentration and methane oxidation (MO_x) rate measurements from the eastern tropical north Pacific (ETNP) water column. This region comprises low-CH₄ waters and a depth interval (~200–760 m) of CH₄ supersaturation that is located within a regional oxygen minimum zone (OMZ). MO_x rate measurements were made in parallel using tracer-based methods with low-level ¹⁴C-CH₄ (LL ¹⁴C) and ³H-CH₄ (³H). The two tracers showed similar trends in MO_x rate with water depth, but consistent with previous work, the LL ¹⁴C rates (range: 0.034–15 × 10⁻³ nmol CH₄ L⁻¹ d⁻¹) were systematically slower than the parallel ³H rates (range: 0.098–4000 × 10⁻³ nmol CH₄ L⁻¹ d⁻¹). Priming and background effects associated with the ³H-CH₄ tracer and LL ¹⁴C filtering effects are implicated as the cause of the systematic difference. The MO_x rates reported here include some of the slowest rates measured in the ocean to date, are the first rates for the ETNP region, and show zones of slow CH₄ turnover within the OMZ that may permit CH₄ derived from coastal sediments to travel great lateral distances. The MO_x rate constants correlate with both CH₄ and oxygen concentrations, suggesting that their combined availability regulates MO_x rates in the region. Depth-integrated MO_x rates provide an upper limit on the magnitude of regional CH₄ sources and demonstrate the importance of water column MO_x, even at slow rates, as a sink for CH₄ that limits the ocean-atmosphere CH₄ flux in the ETNP region.

1. Introduction

Methane (CH₄) is a powerful greenhouse gas that plays important roles in atmospheric chemistry [Cicerone and Oremland, 1988]. The marine environment constitutes a vast reservoir of CH₄ (>10¹⁹ g carbon) [Dickens, 2003; Zhang et al., 2011], but due to highly efficient and microbially mediated CH₄ oxidation, very little marine CH₄ makes its way to the atmosphere. Current estimates indicate that only 4–15 Tg CH₄ yr⁻¹, or 0.7–2.7% of the annual total sources of atmospheric CH₄, come from ocean-atmosphere exchange [Houweling et al., 2000; Wuebbles and Hayhoe, 2002; Denman et al., 2007; Ciais et al., 2013]. Thus, aerobic and anaerobic CH₄ oxidation together nearly balance CH₄ production in the marine environment and act as a “cap” that limits the influence of this large CH₄ reservoir on the atmosphere [Reeburgh, 2007]. However, many aspects of the marine CH₄ budget are not well understood or quantified. For example, the estimates of total CH₄ oxidation in ocean waters and shallow sediments that are used to constrain marine sources range between 75 and 304 Tg CH₄ yr⁻¹ [Hinrichs and Boetius, 2002; Reeburgh, 2007]. Furthermore, the effects of environmental factors that can regulate the rate of CH₄ oxidation, including nutrient availability, temporal variations in CH₄ concentrations, and oxygen levels, are not well quantified. This lack of quantitative understanding limits the ability to estimate how past and future climate may have altered the role of the ocean as a source or sink for atmospheric CH₄.

Few measurements of CH₄ oxidation rates exist for oxic ocean waters (MO_x), and the overall consumption of marine CH₄ by this process is less studied than anaerobic CH₄ oxidation [Reeburgh, 2007]. The available MO_x rate measurements span several orders of magnitude (~0.001–10 nmol CH₄ L⁻¹ d⁻¹) and are insufficient to reveal the environmental factors that regulate MO_x [Mau et al., 2013]. An especially important, yet unresolved issue is whether oxidation ceases when CH₄ levels reach a threshold too low to support a microbial community [Scranton and Brewer, 1978; Valentine et al., 2001; Heeschen et al., 2004; Mau et al., 2013]. Central (i.e., noncoastal) surface and deep ocean waters typically have low-CH₄ concentrations (<1–5 nmol L⁻¹), and MO_x rates in these waters are therefore expected to be slow and difficult to measure accurately. Turnover times of

14–50 years (and longer for water masses >150 years old) have been estimated for the deep ocean using water mass age and CH₄ concentrations [Scranton and Brewer, 1978; Rehder et al., 1999; Heeschen et al., 2004; Keir et al., 2005]. These are quite long compared to turnover times of 5–15 days measured in waters where active CH₄ seepage occurs [de Angelis et al., 1993; Pack et al., 2011; Heintz et al., 2012]. The large volume of low-CH₄ waters in the central and deep ocean means that even slow MO_x rates in these waters can provide an important sink in the overall marine CH₄ budget.

One reason for the lack of MO_x rate measurements in oxic ocean waters is the challenge of measuring slow rates at low-CH₄ concentrations. Methanotrophs, bacteria capable of using CH₄ as their sole source of carbon and energy, oxidize CH₄ in oxic waters via the net reaction:



MO_x rates are measured by adding ¹⁴C-CH₄ or ³H-CH₄ tracer to water samples, incubating the samples for a given period of time, then removing the unreacted CH₄ and quantifying the amount of tracer that accumulated in the products. Well-established tracer-based methods for the direct measurement of MO_x rates use ¹⁴C-CH₄ or ³H-CH₄ tracer at high levels (abbreviated as HL ¹⁴C and ³H); they use 10⁵ Bq per 160 mL of water and measure the conversion of the CH₄ tracer to carbon dioxide (CO₂) and cell biomass (HL ¹⁴C tracer) or water (³H tracer) by decay counting [Ward et al., 1987; Valentine et al., 2001; Heintz et al., 2012]. However, to detect the resulting radioactivity in the products requires a minimum addition of CH₄ tracer to the water sample (background seawater by decay counting is ~50 Bq per 160 mL). The addition of tracer to the typical volume of water utilized (160 mL) raises CH₄ concentrations by ~2–10 nmol L⁻¹ for ³H, and ~400 nmol L⁻¹ for HL ¹⁴C [Mau et al., 2013; Valentine et al., 2001]. In the open and deep ocean regions where CH₄ concentrations are 5 nmol L⁻¹ or lower, these levels of tracer addition raise the amount of CH₄ significantly (>100 times for HL ¹⁴C), possibly accelerating the measured MO_x rates through priming [Ward et al., 1987]. Further, the interaction of the ³H-CH₄ radioactive decay (which has a 12.3 years half-life compared to 5730 years for ¹⁴C-CH₄) with surrounding molecules and ³H-CH₄ isotope exchange (a process not observed with ¹⁴C-CH₄ tracers) can lead to high ³H method backgrounds. These backgrounds are not well quantified and may become significant at slow MO_x rates. A recently developed low-level ¹⁴C-CH₄ method (LL ¹⁴C) [Pack et al., 2011] that raises CH₄ concentrations in samples by only 0.004 nmol L⁻¹, uses ~10⁶ times less radioactivity and accelerator mass spectrometry (AMS) to measure radioactivity, addresses the challenge of MO_x rate measurements in low-CH₄ waters (background seawater by AMS is on the order of 0.001 Bq per 160 mL). A previous comparison of the ³H and LL ¹⁴C methods in coastal waters demonstrated good agreement at rates faster than 0.1 nmol CH₄ L⁻¹ d⁻¹, but at slower rates the LL ¹⁴C results were systematically lower than the ³H results [Pack et al., 2011]. Additional LL ¹⁴C and ³H comparisons along with controlled experiments are needed to continue establishing the LL ¹⁴C method.

In this study, we applied the LL ¹⁴C and ³H tracer methods to measure MO_x rates in the low-CH₄ waters of the eastern tropical north Pacific (ETNP). The ETNP is an area of high, upwelling-derived surface productivity that generates large quantities of sinking organic matter [Pennington et al., 2006]. Respiration of the organic matter as it descends through the water column, combined with poor ventilation, forms a regional oxygen minimum zone (OMZ) centered near 400 m depth [Pennington et al., 2006]. The OMZ extends more than 1500 km off the Mexican coast and covers an approximate area of 5.2 × 10⁶ km² (Figure 1) [Sansone et al., 2001]. Methane concentrations in the OMZ are 79 nmol L⁻¹ at the Mexican coast and >10 nmol L⁻¹ hundreds of kilometers off the coast [Sansone et al., 2001, 2004]. Overall, the ETNP comprises the largest reported open ocean CH₄ pool (~0.3 Tg CH₄) and the OMZ provides a local maximum in CH₄ compared to open ocean surface waters of ~2–8 nmol L⁻¹ and deep ocean background waters of ~2–3 nmol L⁻¹ [Sansone et al., 2001].

Past studies of CH₄ dynamics in the ETNP region indicate that CH₄ found within the OMZ has two probable sources: CH₄ produced in situ and CH₄ advected from coastal sediments. Methane in the upper 200–400 m has depleted δ¹³C-CH₄ values (–45‰ to –42‰) that point to a lightly oxidized biogenic source [Sansone et al., 2001]. Hence, it is thought that shallow CH₄ is locally produced in the anaerobic microenvironments of sinking particles and organisms' intestinal tracts, or from the decomposition of methylphosphonates as a metabolic by-product [Karl and Tilbrook, 1994; Sansone et al., 2001; Reeburgh, 2007;

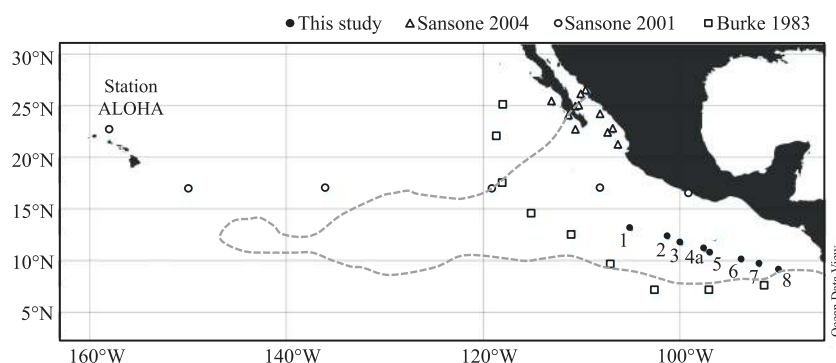


Figure 1. Map of the ETNP (eastern tropical north Pacific) region produced via Ocean Data View software (Schlitzer [2010]) and showing the stations occupied for this study (closed circles, numbered 1–8) and the location of past studies on methane dynamics in the region. The previous studies include Sansone *et al.* [2004] (open triangles), Sansone *et al.* [2001] (open circles), and Burke *et al.* [1983] (open squares). The dashed gray line is the OMZ area defined by Sansone *et al.* [2001] where the oxygen is $9 \mu\text{mol L}^{-1}$ at 400 m. Station ALOHA is the location of ongoing time series experiments [Karl, 1999].

Karl *et al.*, 2008]. Methane below 400 m is enriched in ^{13}C (-26‰ to -30‰) near the coast and becomes even more enriched with distance from the coast ($10\text{--}15\text{‰}$) [Holmes *et al.*, 2000; Sansone *et al.*, 2001]. Microbial CH_4 oxidation preferentially uses $^{12}\text{C}\text{-CH}_4$ and leaves the residual CH_4 enriched in ^{13}C [Coleman *et al.*, 1981]. Thus, the deeper pool is believed to be CH_4 that was moderately oxidized within the OMZ while advecting from organic-rich coastal sediments to the open ocean (>1500 km). The low O_2 conditions in the OMZ are hypothesized to slow MO_x and allow CH_4 to travel long distances [Sansone *et al.*, 2001, 2004].

While a number of studies have focused on CH_4 dynamics in the ETNP region [Burke *et al.*, 1983; Holmes *et al.*, 2000; Sansone *et al.*, 2001, 2004], to date no direct measurements of MO_x rates have been reported and the hypotheses those studies generated about low MO_x in the OMZ or how MO_x affects the potential flux of CH_4 from ocean to atmosphere in this region remain untested. A number of similar oxygen minimum zones exist in the marine environment and these zones may expand in response to changes in ocean circulation and anthropogenic macronutrient inputs [Naqvi *et al.*, 2010]. A sound understanding of CH_4 dynamics in oxygen minimum zones will be essential in predicting potential future changes in CH_4 pool size and CH_4 emissions from these zones [Naqvi *et al.*, 2010].

2. Methods

2.1. Sampling

Samples were collected inside the ETNP (Figure 1) during a December 2008 cruise aboard the R/V *Knorr*. Water samples were collected in 10 L Niskin bottles attached to a Rosette with a conductivity-temperature-depth (CTD) package (Sea-bird SBE 9) from eight stations in the ETNP (Figure 1 and Table 1). Samples for CH_4 concentration and $^3\text{H}\text{-CH}_4$ oxidation rate measurements were transferred directly from the Niskin

bottles to 160 mL glass serum bottles (Wheaton No. 223748) using Tygon tubing. The bottles were filled from the bottom, flushed with two volumes of water, and sealed with gray butyl stoppers (Wheaton No. W224100-193) and aluminum crimp caps (Wheaton No. 224178-01). After sealing, each sample was inspected to ensure it was free of bubbles. Two samples from each depth were taken for LL $^{14}\text{C}\text{-CH}_4$ oxidation rate measurements. Samples were taken directly from the Niskin

Table 1. Stations Occupied in the ETNP Region During This Study

| Station | Latitude ($^{\circ}\text{N}$) | Longitude ($^{\circ}\text{W}$) |
|---------|---------------------------------|----------------------------------|
| 1 | 13.023 | 104.992 |
| 2 | 12.232 | 101.229 |
| 3 | 11.624 | 99.845 |
| 4a | 11.009 | 97.480 |
| 5 | 10.69 | 96.944 |
| 6 | 9.999 | 93.722 |
| 7 | 9.521 | 91.954 |
| 8 | 8.999 | 90.001 |

bottles in 120 mL glass serum bottles (Wheaton No. 223747) previously washed with methanol, 5% hydrochloric acid, and then deionized water. The bottles were rinsed three times with sample water, filled from the bottom to overflowing using Tygon tubing and then sealed as described above. MO_x rate measurements were made at all stations occupied using the $^3\text{H-CH}_4$ tracer but only at Stations 1, 3, 6, and 8 (Figure 1) with the LL $^{14}\text{C-CH}_4$ tracer, because the method required more processing time per sample.

2.2. Analytical Methods

2.2.1. Oxygen and Methane Concentrations

Measurements of O_2 concentration were made with an SBE 43 sensor on the CTD package and verified with Winkler titrations throughout the cruise. After collection, samples for CH_4 concentration analysis were killed with 0.5 mL of aqueous saturated mercuric chloride solution and shaken vigorously. Then, a 10 mL headspace of ultrahigh-purity nitrogen gas (UHP N_2) was introduced by displacement of an equivalent amount of water. Finally, samples were placed upside down in boxes to prevent gas leakage through sample stoppers during transport and storage. On shore, the sample headspaces were analyzed for CH_4 concentration in two 3 mL aliquots using a gas chromatograph equipped with a flame ionization detector (GC 14A; Shimadzu). The results were corrected for the amount of CH_4 still dissolved in solution with Bunsen solubility coefficients [Yamamoto *et al.*, 1976] calculated from room temperature at the time of analysis and sample salinity. The precision based on duplicate samples was on average $\pm 11\%$. Air-equilibrated CH_4 solubility was estimated using the Yamamoto *et al.* [1976] Bunsen coefficients based on in situ salinity and potential temperature and an atmospheric CH_4 mixing ratio of $1.8 \mu\text{L L}^{-1}$. Percent saturation was calculated by comparing the measured CH_4 concentrations to the air-equilibrated concentrations.

2.2.2. $^3\text{H-CH}_4$ Oxidation Rate Measurements

MO_x rate measurements with the $^3\text{H-CH}_4$ tracer were made as described in Valentine *et al.* [2001] and Heintz *et al.* [2012]. In a shipboard radiation van, the 160 mL water samples were injected with 50 μL aliquots of $^3\text{H-CH}_4$ (370 kBq, 6360 kBq mg^{-1} tracer, 4 $\mu\text{mol L}^{-1}$ CH_4 in N_2 ; American Radiolabeled Chemicals) and incubated in the dark for 24 h. Samples were incubated in a refrigerator (6°C), an incubator with temperature control (13–19°C) or at room temperature regulated by air conditioning (21°C). Temperature was measured with an alcohol thermometer kept with the incubating samples and recorded at the start of the incubations. After incubations were complete, the stoppers and 60 mL of water were removed from the sample bottles, and samples were sparged with UHP N_2 for 30 min to remove unreacted CH_4 . Finally, samples were resealed and stored for transport back to shore.

In a shore-based laboratory, the quantity of $^3\text{H-H}_2\text{O}$ in each sample was measured by liquid scintillation counting. Procedure blanks were determined by counting untreated seawater, and the blank values were subtracted from the rate samples. A fractional turnover rate (k) was calculated by dividing the fraction of $^3\text{H-CH}_4$ tracer that was converted to $^3\text{H-H}_2\text{O}$ by the incubation time. MO_x rates (R_{oxd}) were calculated as the product of k and the in situ CH_4 concentration ($[\text{CH}_4]$) assuming first-order kinetics:

$$R_{\text{oxd}} = k \times [\text{CH}_4] \quad (1)$$

Methane turnover times (τ) with respect to oxidation were calculated as the inverse of k :

$$\tau = 1/k \quad (2)$$

Killed controls were taken (1–2 per CTD cast) to spot check that nonbiological processes did not incorporate the $^3\text{H-CH}_4$ tracer into the aqueous phase and to test for impurities in the $^3\text{H-CH}_4$ that may remain in the samples after purging. Killed controls were treated with 0.1 mL of aqueous saturated mercuric chloride solution prior to injection with $^3\text{H-CH}_4$ and then subjected to the procedures outlined above.

2.2.3. Low-Level $^{14}\text{C-CH}_4$ Oxidation Rate Measurements

Preparation and Activity of the LL $^{14}\text{C-CH}_4$ Tracer and $^{14}\text{C-Free CO}_2$. A diluted form of the $^{14}\text{C-CH}_4$ tracer used in Pack *et al.* [2011] was employed here; an aliquot of the Pack *et al.* tracer was diluted by a factor of 115 with $^{14}\text{C-free CO}_2$ (Matheson Gas, anaerobic grade) in a preevacuated 6 L stainless canister. The activity of the resulting $^{14}\text{C-CH}_4$ tracer was determined using the methods outlined by Pack *et al.* [2011] and found to be 0.00013 ± 0.00001 kBq per 50 μL of tracer ($5.4 \pm 0.4 \times 10^{-14}$ moles ^{14}C per 50 μL tracer or 0.00139 ± 0.00009 kBq mg^{-1} tracer). The $^{14}\text{C-free CO}_2$ used with background samples was prepared by adding the same CO_2 as used with the tracer (Matheson Gas, anaerobic grade) to a preevacuated 2 L stainless canister.

Shipboard ^{14}C Labeling. Samples for LL ^{14}C rate measurements were processed using a modified version of the method described in Pack *et al.* [2011] and in a separate radiation van from that used for the ^3H measurements. The equipment used with the ^3H rate samples had previously been exposed to HL ^{14}C tracers, so in order to avoid contamination of the LL ^{14}C samples with residual HL ^{14}C tracer, it was important to completely separate the processing of the ^3H and LL ^{14}C samples. One of the two 120 mL water samples collected from each depth was injected with 50 μL of $^{14}\text{C}\text{-CH}_4$ (0.00013 kBq, 0.00139 kBq mg^{-1} tracer, 0.0086 $\mu\text{mol L}^{-1}$ CH_4 in ^{14}C -free CO_2), while the other was treated with 50 μL of pure ^{14}C -free CO_2 . This treatment yielded sets of labeled and background samples. Following injection, samples were shaken to facilitate CH_4 dissolution and incubated in the dark for 36 h. Samples were incubated in a shipboard refrigerator or inside coolers kept at room temperature (regulated by air conditioning). Temperatures were measured and recorded through the entire incubation with temperature data loggers (Onset Computer Corporation No. TBI32-05 + 37).

After incubation, samples were filtered to collect cell biomass, killed, and purged of unreacted CH_4 . For filtering, we used procedures that collected the cell biomass without exposing sample filtrate to atmospheric CO_2 , which can alter the sample $^{14}\text{C}\text{-CO}_2$ content. First, 60 mL of sample was transferred to a syringe by displacement with an equivalent amount of UHP N_2 . Next, a syringe filter holder (EMD Millipore Corporation No. SX0002500) with a 1.2 μm nominal pore size quartz fiber filter (25 mm diameter, SKC No. 225-1824) was attached to the syringe with sample, and the sample was vacuum filtered into a sealed 120 mL serum bottle. The serum bottle receiving the filtrate was previously capped with a gray butyl stopper, purged with UHP N_2 and filled with 0.4 mL of aqueous sodium hydroxide solution (saturated and carbonate free). The sodium hydroxide (NaOH) killed any bacteria in the filtrate and preserved the $^{14}\text{C}\text{-CO}_2$ gas oxidation product as carbonate ions (CO_3^{2-}) in solution. The unreacted CH_4 was then removed from the sample filtrate by purging with UHP N_2 for 40 min. The purging was performed with sealed bottles using two needles: one 16 gauge, 10 cm needle (Air-Tite Products No. N164) inserted into the bottom of the sample bottle to deliver the N_2 , and a 23 gauge, 2.5 cm needle (Fisher Scientific No. 14-826-6B) inserted in the sample headspace as a vent for the stripped gases and N_2 . After purging was complete, the gray butyl sample stoppers were replaced with blue butyl stoppers (Bellco Glass No. 2048-11800) in a homemade glove chamber with UHP N_2 flow. The blue butyl stoppers provided a superior seal for sample transport and storage. The sealed samples were stored upside down in boxes and transported back to shore.

The quartz filters with the cell biomass were partially dried by vacuum, rolled up, and inserted into 5 cm long, 6 mm diameter, prebaked quartz tubes with stainless steel tweezers and completely dried on a 60°C hotplate for 1–2 h. The quartz tubes with dry filters were capped with clean aluminum foil and column caps (Supelco No. 20439), transported back to shore, and stored at -10°C until $^{14}\text{C}\text{-AMS}$ analysis.

Samples for killed controls were collected once per CTD cast to spot check tracer purity, abiotic incorporation of tracer and NaOH killing efficacy. The samples were treated with NaOH before or within 30 min of the $^{14}\text{C}\text{-CH}_4$ injection, incubated, and treated as described above.

Shore-Based $^{14}\text{C}\text{-AMS}$ Analyses. Shore-based measurements quantified the ^{14}C in the dissolved inorganic carbon (DIC: CO_2 , carbonic acid, bicarbonate, and carbonate) and cell biomass that accumulated in samples during incubation with the LL $^{14}\text{C}\text{-CH}_4$ tracer. DIC was extracted from ^{14}C -labeled background and killed control samples and the ^{14}C -content measured at the University of California, Irvine Keck Carbon Cycle AMS facility as described in Pack *et al.* [2011]. However, our ^{14}C -labeled samples did not require dilution with ^{14}C -free CO_2 prior to analysis because they were well below the maximum AMS detection limit (~ 8 times modern under the standard operating conditions at the Keck Carbon Cycle AMS facility). Procedure blanks were determined from a ^{14}C -free DIC standard (calcite in DIC-free seawater) prepared and extracted in parallel with DIC samples and then subtracted from all DIC samples.

The cell biomass on the quartz filters was prepared for $^{14}\text{C}\text{-AMS}$ analysis via double tube combustions. The tubes in which the filters had been stored frozen were cleaned with methanol and placed inside 18 cm long, 9 mm diameter quartz combustion tubes containing 0.28 mg acetanilide, 80 mg cupric oxide, and silver wire (1 mm in diameter, ~ 3 mm long). Acetanilide was used as a dead carbon (^{14}C -free) carrier, because the filters contained < 0.03 mg of carbon, and at least 0.1 mg is necessary for a standard AMS measurement. The combustion tubes containing the filters were evacuated, flame-sealed, and

Table 2. Summary of Incubation Temperatures for the LL ^{14}C and ^3H Rate Samples

| Station | Sample Depth (m) | Number of Samples ^a | Incubation Temperature | |
|---------|------------------|--------------------------------|-------------------------|-------------------|
| | | | LL ^{14}C (°C) | ^3H (°C) |
| 1 | 6–21 | 2 | 23 | 18 |
| 1 | 48–58 | 2 | 23 | 15 |
| 1 | 68–2476 | 14 | 14 | 15 |
| 3 | 5–113 | 7 | 21 | 21 |
| 3 | 132–201 | 2 | 5 | 15 |
| 6 | 26–59 | 3 | 21 | 18 |
| 6 | 73–374 | 4 | 5 | 15 |
| 8 | 22 | 1 | 23 | 18 |
| 8 | 33–264 | 5 | 5 | 13 |
| 8 | 527–2470 | 6 | 8 | 6 |

^aThe number of rate samples that are within the listed depth range.

combusted at 900°C for 2 h. This process quantitatively converted the sample cell biomass and acetanilide to CO_2 , and the CO_2 was prepared for ^{14}C -AMS analysis following the methods outlined in Xu *et al.* [2007]. The ^{14}C values of filters from background samples were averaged and used as a procedure blank for filters with ^{14}C -labeled cell material.

Rate Calculations. The ^{14}C that accumulated in the DIC and cell biomass ($^{14}\text{C}_{\Delta\text{DIC}}$ and $^{14}\text{C}_{\Delta\text{CM}}$, respectively) during incubation with LL ^{14}C - CH_4 tracer was calculated as follows.

$$^{14}\text{C}_{\Delta\text{DIC}} = (^{14}\text{C}_{\text{LDIC}} - ^{14}\text{C}_{\text{BDIC}}) \times \text{DIC} \times V_s \quad (3)$$

$$^{14}\text{C}_{\Delta\text{CM}} = (^{14}\text{C}_{\text{LCM}} - ^{14}\text{C}_{\text{BCM avg}}) \times \text{CO}_2 \times V_s/V_f \quad (4)$$

Here $^{14}\text{C}_{\text{LDIC}}$ and $^{14}\text{C}_{\text{BDIC}}$ are the $^{14}\text{C}:^{12}\text{C}$ ratios of the DIC in the labeled and background samples, respectively; DIC is the sample DIC concentration (ΣCO_2); and V_s is the sample volume. V_f is the volume of sample filtered; CO_2 is the moles of CO_2 recovered from filter combustion with acetanilide; and $^{14}\text{C}_{\text{LCM}}$ and $^{14}\text{C}_{\text{BCM avg}}$ are the $^{14}\text{C}:^{12}\text{C}$ ratios of the cellular material-acetanilide mixture in labeled samples and averaged background samples, respectively. Next, the fractional turnover rate (k) was calculated using the moles of LL ^{14}C - CH_4 added to each sample ($^{14}\text{CH}_4$):

$$k = \frac{(^{14}\text{C}_{\Delta\text{DIC}} + ^{14}\text{C}_{\Delta\text{CM}}) / ^{14}\text{CH}_4}{\text{incubation time}} \quad (5)$$

MO_x rates (R_{oxd}) and turnover times (τ) were calculated according to equations (1) and (2) above. Lastly, the fraction of the ^{14}C - CH_4 consumed that was allocated to cell biomass (P_{CL}) was calculated:

$$P_{\text{CL}} = 100 \times \frac{^{14}\text{C}_{\Delta\text{CM}}}{(^{14}\text{C}_{\Delta\text{DIC}} + ^{14}\text{C}_{\Delta\text{CM}})} \quad (6)$$

2.2.4. Q_{10} Correction for MO_x Rates

Incubation temperature is an important factor in MO_x rate measurements [Heintz, 2011], and every effort was made to incubate parallel-processed LL ^{14}C and ^3H samples at the same temperature and near in situ temperatures. Nonetheless, a malfunctioning internal thermometer and limited refrigerator/incubator facilities in the radiation vans aboard ship resulted in some significant differences. As summarized in Table 2, incubation temperature differences for parallel LL ^{14}C and ^3H samples ranged from 0 to 10°C. Differences between in situ and incubation temperatures were 0 to 12°C (median: 5°C) for both the LL ^{14}C and ^3H samples. In an effort to account for these differences and present rates that are more representative of in situ conditions, we used a Q_{10} calculation to estimate what each LL ^{14}C and ^3H rate would be, had samples been incubated exactly at in situ temperatures (see equation (S1) and Text S1 in the supporting information for the calculation details). The corrections to our rates ranged from a factor of 1 (no correction) to 2.4, with a median of 1.5, and only a few samples were corrected by a factor >2. We present only the Q_{10} -corrected rates in sections 3 and 4 below.

3. Results

3.1. Dissolved Oxygen, Methane Concentrations and MO_x Rates

Dissolved oxygen profiles (Figures 2 and 3) show an OMZ, centered around 400 m depth that is typical for the ETNP region [Burke *et al.*, 1983; Sansone *et al.*, 2001]. Oxygen levels were saturated in surface waters and decreased below the mixed layer to $2 \mu\text{mol L}^{-1}$ by 300 m depth. The OMZ extended to ~750–800 m depth, with O_2 levels increasing in deeper waters (Figure 3).

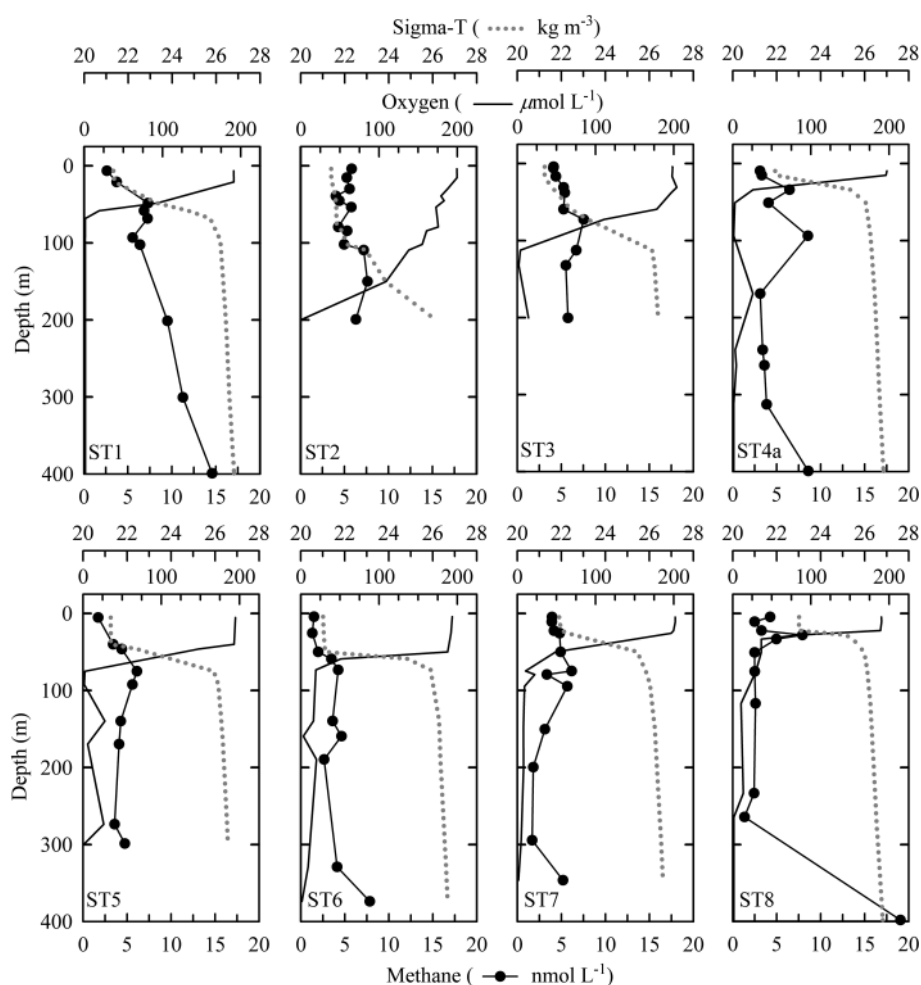


Figure 2. Profiles of methane, oxygen, and sigma-t in the upper 400 m of the water column for Stations 1–8.

Methane concentration profiles (Figures 2 and 3) had two consistent features. The first was a subsurface maximum typical of open ocean waters [Lamontagne *et al.*, 1973; Burke *et al.*, 1983; Reeburgh, 2007] with CH_4 concentrations of $4.6\text{--}7.9\text{ nmol L}^{-1}$ (189–367% supersaturated with respect to the atmosphere). The second feature was a midwater maximum centered in the OMZ with CH_4 concentrations of 8.6 to 19 nmol L^{-1} (317–709% supersaturated) and observed in previous studies [Burke *et al.*, 1983; Sansone *et al.*, 2001, 2004]. At Station 1, the midwater maximum extended into the subsurface maximum, whereas at Station 8 the two maxima were well separated. This suggests that the midwater maximum may influence CH_4 in the mixed layer and surface waters in some areas of the ETNP. Below the OMZ ($>750\text{--}800\text{ m}$), CH_4 concentrations transitioned to undersaturated levels and reached a minimum value of 0.27 nmol L^{-1} (8% saturated).

The MO_x rates in this study ranged from 0.000034 to $0.015\text{ nmol CH}_4\text{ L}^{-1}\text{ d}^{-1}$ for the LL ^{14}C method and $0.000098\text{--}4.0\text{ nmol CH}_4\text{ L}^{-1}\text{ d}^{-1}$ for the ^3H method. Profiles of MO_x rates (Figures 4 and 5) showed highest values near the subsurface CH_4 maximum: the LL ^{14}C rates increased to $0.0016\text{--}0.015\text{ nmol CH}_4\text{ L}^{-1}\text{ d}^{-1}$, while the ^3H rates reached $0.17\text{--}4.0\text{ nmol CH}_4\text{ L}^{-1}\text{ d}^{-1}$. Higher MO_x rates were also present in the OMZ near the midwater CH_4 maximum, with rates reaching $0.010\text{--}0.012\text{ nmol CH}_4\text{ L}^{-1}\text{ d}^{-1}$ and $0.048\text{--}0.17\text{ nmol CH}_4\text{ L}^{-1}\text{ d}^{-1}$ for the LL ^{14}C and ^3H methods, respectively. These higher MO_x rates were bounded, above and below, with lower MO_x rates that reached minimum values of $0.00022\text{ nmol CH}_4\text{ L}^{-1}\text{ d}^{-1}$ (LL ^{14}C) and $0.0019\text{ nmol CH}_4\text{ L}^{-1}\text{ d}^{-1}$ (^3H). Below the OMZ, MO_x rates slowed to $<0.00046\text{ nmol CH}_4\text{ L}^{-1}\text{ d}^{-1}$ (LL ^{14}C) and $<0.12\text{ nmol CH}_4\text{ L}^{-1}\text{ d}^{-1}$ (^3H).

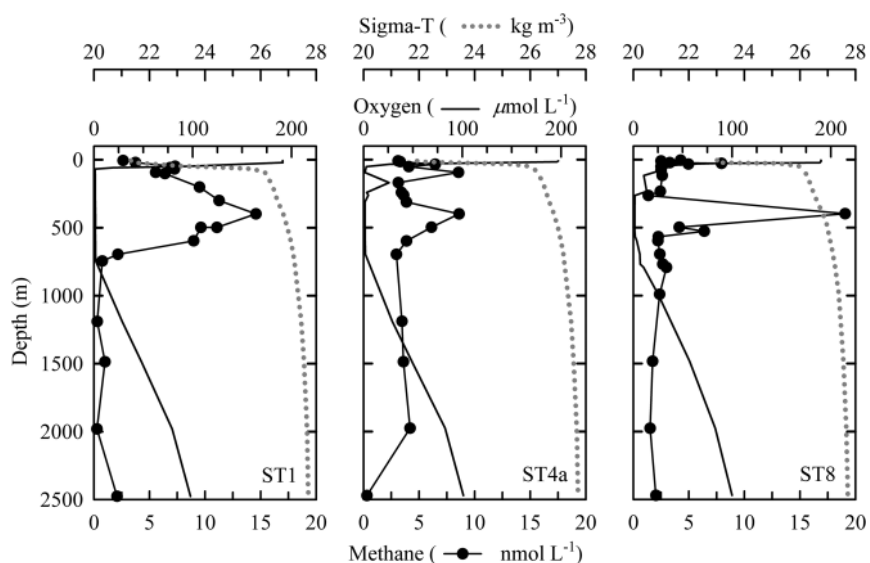


Figure 3. Profiles of methane, oxygen, and sigma-t down to 2500 m in the water column for Stations 1, 4a, and 8.

The fraction of $^{14}\text{C}\text{-CH}_4$ allocated to cell biomass (P_{CL} , equation (6)) ranged from 0.52% to 7.8% in 10 samples with turnover times <700 days (τ , equation (2)) but was not detectable in other samples with longer turnover times. The quartz filters containing the cell biomass must have $>4 \times 10^{-19}$ moles ^{14}C for the AMS analysis used here, and filters from samples with turnover times >700 days did not contain enough ^{14}C .

3.2. Comparison of the Low-Level $^{14}\text{C}\text{-CH}_4$ and $^3\text{H}\text{-CH}_4$ Rates

As is readily apparent, the two tracer methods, although yielding similar patterns of MO_x rates with depth, differed in absolute values. The MO_x rates obtained with LL ^{14}C were systematically lower than those measured using ^3H (Figures 4 and 5). Forty-four of the LL ^{14}C rates were 2–184 (median: 16) times slower than the parallel ^3H rates, while one LL ^{14}C rate was 1.6 times faster (Figure 6).

3.3. Duplicate and Killed Control Rate Samples

The mean coefficient of variation from ^3H rate measurements on 112 pairs of duplicate samples was 18% (range: 0.6–91%). For the LL ^{14}C rate measurements, 10 pairs of duplicate samples gave a mean coefficient of variation of 10% (range: 0.2–36%). The error associated with each method was also estimated by combining analytical errors from sample processing (e.g., decay counting, $^{14}\text{C}\text{-AMS}$, procedure blanks, sample volume, etc.) in error propagation equations. These analytic errors, withstanding the Q_{10} correction, were on average 17% for both the ^3H and LL ^{14}C methods for the range of rates measured with each method in this study. Incorporating the Q_{10} error in the propagation is not straightforward because of method artifacts and unanticipated variability in incubation temperatures attributed to incubator cooling cycles (see supporting information Text S1). Nevertheless, a conservative estimate of propagated error including the Q_{10} correction gives an average error of 56% (^3H) and 59% (LL ^{14}C).

Killed control samples from the ^3H rate measurements yielded rates that were 0.2–9.4% of their corresponding rate samples and are consistent with past studies [Valentine *et al.*, 2001; Heintz *et al.*, 2012]. LL ^{14}C killed control samples yielded rates that were 13–64% of their corresponding rate samples, and killed controls that were poisoned with NaOH 2–33 min after injection with $^{14}\text{C}\text{-CH}_4$ tracer showed higher rates than those killed before injection. These high killed controls show that microbial activity in samples was not completely stopped when the $^{14}\text{C}\text{-CH}_4$ was added and that NaOH in killed controls must be introduced well before the $^{14}\text{C}\text{-CH}_4$ tracer. Abiotic uptake of $^{14}\text{C}\text{-CH}_4$ tracer or impurities in the tracer could also cause high killed controls, but previous work with the same batch of $^{14}\text{C}\text{-CH}_4$ tracer [Pack *et al.*, 2011] excludes this possibility.

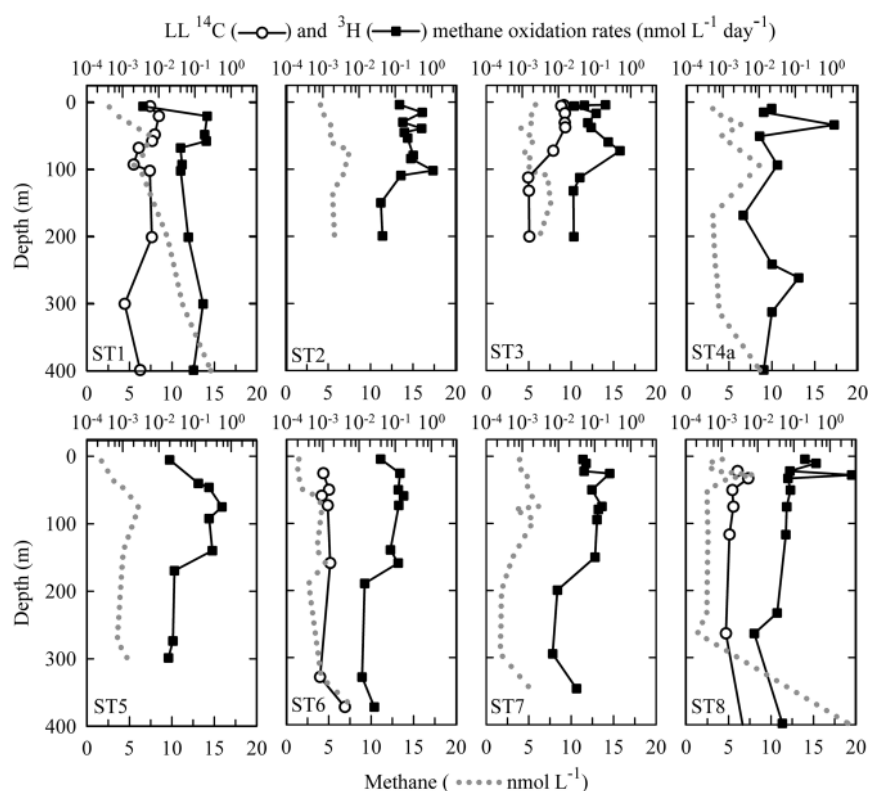


Figure 4. Profiles of methane, and LL ^{14}C and ^3H MO_x rates in the upper 400 m of the water column for Stations 1–8. The error bars for the LL ^{14}C rates are combined analytic errors. The error bars on the ^3H rates are a fixed 18% error based on duplicate samples taken during this study. The error bars for both measurements mostly lie within the data symbols and do not include error from the Q_{10} correction.

4. Discussion

4.1. Performance of the LL ^{14}C - CH_4 and ^3H - CH_4 Methods

The MO_x rates we report here (0.000034 – $4.0 \text{ nmol CH}_4 \text{ L}^{-1} \text{ d}^{-1}$) include some of the lowest rates measured in the marine environment (the bulk of previously reported rates are ~ 0.001 – $10 \text{ nmol CH}_4 \text{ L}^{-1} \text{ d}^{-1}$) [Mau *et al.*, 2013]. Also, the systematic difference between the LL ^{14}C and ^3H parallel rate measurements reported here (i.e., LL $^{14}\text{C} < ^3\text{H}$ rates) is consistent with the previous study where these methods were compared in coastal waters [Pack *et al.*, 2011]. In that study, the two tracer methods were in agreement when MO_x rates were above $0.1 \text{ nmol CH}_4 \text{ L}^{-1} \text{ d}^{-1}$ but diverged when below, with LL ^{14}C rates consistently slower than ^3H rates. In this study, the LL ^{14}C rates ranged from 0.000034 to $0.015 \text{ nmol CH}_4 \text{ L}^{-1} \text{ d}^{-1}$ and were well below the $0.1 \text{ nmol CH}_4 \text{ L}^{-1} \text{ d}^{-1}$ mark reported in the previous study.

The fraction of LL ^{14}C tracer converted to cell biomass (P_{CL} , equation (6)) reported here (0.52%–7.8%) was low compared to some previous studies in the marine environment. Using the HL ^{14}C - CH_4 tracer, previous studies have reported P_{CL} values of 2%–66% [Griffiths *et al.*, 1982; Ward *et al.*, 1987; de Angelis *et al.*, 1993], with one study reporting a maximum P_{CL} of 80% [Ward *et al.*, 1989]. These studies used filters with smaller pore sizes of 0.2–0.45 μm (compared to our 1.2 μm), so some of our low P_{CL} values may have been due to cells that passed through our filters. However, another HL ^{14}C study in low- CH_4 open ocean waters was unable to detect ^{14}C in the cell fraction of any of their samples via 0.45 μm pore size filters [Jones, 1991], indicating that P_{CL} values can vary greatly between environments.

Priming and method backgrounds associated with the ^3H - CH_4 tracer likely led to falsely high ^3H rates at ETNP conditions (see section 1) and contributed to the systematic difference between our ^3H and LL ^{14}C parallel rates. Because the LL ^{14}C method was specifically designed for low- CH_4 waters with slow MO_x rates, it

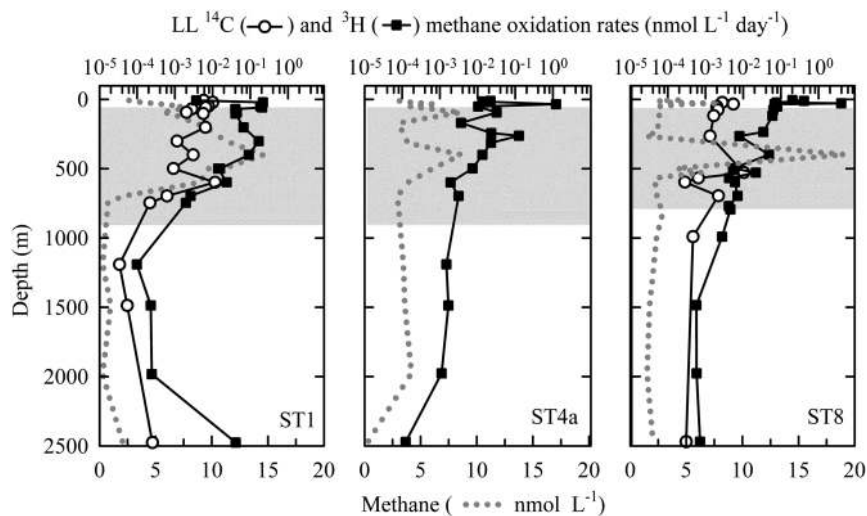


Figure 5. Profiles of methane, and LL ¹⁴C and ³H methane oxidation rates down to 2500 m in the water column for Stations 1, 4a, and 8. The error bars for the LL ¹⁴C and ³H rates are the same as in Figure 4, and the gray boxes show the OMZ depth interval bounded by 10 μmol O₂ L⁻¹.

adds ~300 times less CH₄ to samples and uses ~10⁶ times less radioactivity than the ³H method. This obviates concerns about priming and background effects. Incubation temperature is also an important factor in parallel rate mismatch [Pack *et al.*, 2011], but we made a Q₁₀ correction to the rate data to account for this issue (see section 2). In this study specifically, the large filter pore size (1.2 μm) may have led to falsely low LL ¹⁴C rates and also contributed to the systematic difference between our parallel rates. However, this effect at its *maximum* (assuming zero incorporation of tracer into cells, when it should have been 66%) would have reduced the LL ¹⁴C rate values by a factor of 3. This cannot account for the maximum 184-fold difference (or even the median 16-fold difference) obtained between the two methods.

The combination of the parallel LL ¹⁴C and ³H rates from this study and the previous coastal study show a well-defined trend, albeit with some scatter, of a greater difference between methods at slower MO_x rates (Figure 6). Disagreement between parallel rate measurements has also been reported for the HL ¹⁴C-CH₄ and ³H-CH₄ tracers. A study in the Black Sea reported HL ¹⁴C rates that were 0.1–350 (median: 2.1)

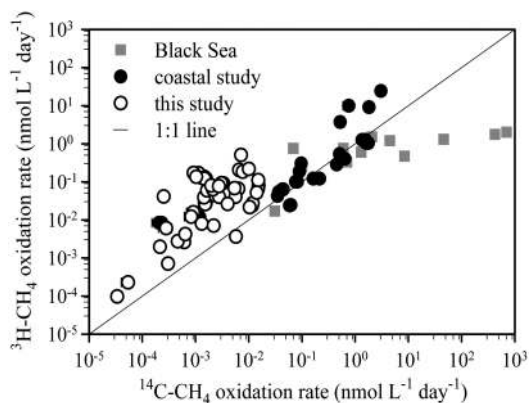


Figure 6. ³H oxidation rates plotted against the corresponding parallel LL ¹⁴C rates from this study and the previous coastal study [Pack *et al.*, 2011]. Parallel rates using HL ¹⁴C and ³H in the Black Sea water column [Reeburgh *et al.*, 1991] are also plotted. Error bars for the LL ¹⁴C and ³H rates from this study are the same as in Figure 4.

times faster than the parallel ³H rates (Figure 6, data from Reeburgh *et al.* [1991]). A more recent study in an Arctic fjord observed ³H rates > HL ¹⁴C rates in ~80 nmol L⁻¹ CH₄ waters, but HL ¹⁴C rates > ³H rates in waters with 20 nmol L⁻¹ CH₄ [Mau *et al.*, 2013]. The study suggested that the 440–540 nmol L⁻¹ increase in CH₄ from the HL ¹⁴C tracer (as opposed to the 1–2 nmol L⁻¹ increase from the ³H tracer) led to priming in the 20 nmol L⁻¹ CH₄ waters. While in the 80 nmol L⁻¹ waters, the enzyme machinery associated with MO_x was apparently at a lower concentration than in the 20 nmol L⁻¹ waters and became saturated with CH₄ from the HL ¹⁴C tracer addition. This situation yielded ³H rates > HL ¹⁴C rates (see the discussion in Mau *et al.* [2013]).

When planning future water column MO_x rate measurements, the ³H, LL ¹⁴C, and HL ¹⁴C methods are all available tools, and their respective strengths and weaknesses should be considered.

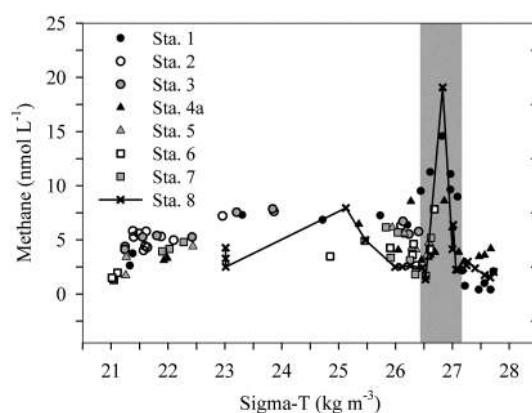


Figure 7. Methane concentrations versus density showing that the midwater CH_4 maximum at different stations falls on a similar density surface highlighted in gray.

The advantage of the ^3H method is that samples can quickly be prepared and rapidly analyzed with liquid scintillation counting; however, it requires specialized radioisotope facilities (radiation vans) in the field. By contrast, the LL^{14}C method avoids the use of radiation vans but is costlier and requires more laboratory processing time than the ^3H method. Taking these strengths and weakness together, the ^3H method is best for surveys where elevated rates are anticipated, radiation vans are available, and a large number of samples need to be processed quickly, while the LL^{14}C method is more appropriate for surveys where priming is a concern and high-level radioactive tracers are not practical due to a lack of radioisotope facilities (remote field sites and rapid response situations).

An additional advantage of the LL^{14}C method is that it can be used to determine the partitioning of methane-carbon between CO_2 and cell biomass (the ^3H method cannot accomplish this). Carbon (C) partitioning provides valuable data for C-cycle studies and for establishing C budgets. The HL^{14}C method can also provide C-partitioning data, its sample processing time lays between the ^3H and LL^{14}C methods (due to filtering and CO_2 collection steps), it is costwise similar to the ^3H method, but it requires a radiation van and has the greatest potential for priming samples. Thus, its most practical use is in high- CH_4 waters where C partitioning is of interest and radiation vans are available.

The rate measurements reported here are the first available from the ETNP region and include some of the lowest reported for the ocean. In the subsequent discussion of ETNP CH_4 dynamics, we will assume the parallel ^3H and LL^{14}C rate data bracket the actual range of MO_x rates, with the LL^{14}C as the minimum (underestimate due to loss of biomass through large pore size filters) and the ^3H data as the maximum (overestimate due to priming and method backgrounds). While this leads to large ranges that are especially noticeable when rates are integrated to a regional scale, it also highlights the large uncertainties in our current understanding of ocean CH_4 budgets.

4.2. ETNP Environmental Controls on Methane and MO_x Rates

Previous studies on CH_4 dynamics in the ETNP region have suggested that low O_2 concentrations limit MO_x in the OMZ, thereby allowing coastal CH_4 to laterally advect long distances to the open ocean [Sansone *et al.*, 2001, 2004]. Two aspects of our rate measurements support this idea. First, minima in MO_x rates within the OMZ (Figure 5) show long turnover times: 2.8–33 years and 0.3–5.5 years for the LL^{14}C and ^3H methods, respectively. Second, average turnover times (τ , equation (1)) for OMZ waters (200–760 m) are 12 years (LL^{14}C) or 1.2 years (^3H) and are longer than the average 4.5 years (LL^{14}C) and 0.3 years (^3H) values in surface waters (5–200 m). Further evidence supporting offshore advection of CH_4 within the OMZ can be found in the relationship between CH_4 concentration and water density (Figure 7); the midwater CH_4 maximum at Stations 1, 4a, and 8, are all near the 26.8 kg m^{-3} isopycnal. This suggests that CH_4 supplying the maximum is advected on a common density surface, possibly from organic-rich coastal sediments in contact with the OMZ.

Our LL^{14}C and ^3H rate data show relationships with a number of environmental parameters and provide insight into the controls on MO_x rates in ETNP waters. LL^{14}C fractional turnover rates (k) show weak, but statistically significant ($p < 0.05$) linear correlations with the product of CH_4 and O_2 concentrations ($\text{CH}_4 \times \text{O}_2$), O_2 , temperature, salinity, and density (Table 3). ^3H values of k show statistically significant, although weaker, linear correlations with O_2 , temperature, salinity, and density (Table 3). The strongest linear correlation appears between the LL^{14}C values of k and $\text{CH}_4 \times \text{O}_2$ ($r^2 = 0.67$, $\text{df} = 43$, Figure 8 and Table 3). This suggests that the combined availability of CH_4 and O_2 (i.e., second-order kinetic control) may influence MO_x rates in the ETNP region.

Table 3. Summary of Linear Regression Analyses Between LL ¹⁴C or ³H Fractional Turnover Rate (*k*) and Environmental Parameters (Degrees of Freedom, df = 43)

| Parameter | LL ¹⁴ C <i>k</i> (d ⁻¹) | | | ³ H <i>k</i> (d ⁻¹) | | |
|---|--|-----------------------|----------|--|--|-----------------------|
| | Slope × 10 ⁻⁵ | <i>r</i> ² | <i>p</i> | Slope × 10 ⁻⁵ | (<i>r</i> ²) ^a | <i>p</i> ^b |
| CH ₄ × O ₂ (nmol L ⁻¹ × μmol L ⁻¹) | 0.13 | 0.67 | <0.0001 | 0.8 | 0.11 | 0.026 |
| CH ₄ (nmol L ⁻¹) | 2.0 | 0.00 | 0.84 | -7.8 | 0.02 | 0.37 |
| O ₂ (μmol L ⁻¹) | 0.46 | 0.54 | <0.0001 | 4.3 | 0.22 | 0.0011 |
| Temperature (°C) | 4.3 | 0.54 | <0.0001 | 66 | 0.32 | <0.0001 |
| Salinity | -70 | 0.49 | <0.0001 | -540 | 0.25 | 0.0005 |
| Density (sigma-theta, kg m ⁻³) | -17 | 0.61 | <0.0001 | -210 | 0.32 | <0.0001 |

^aThe coefficient of determination for each linear regression.

^b*P* value to evaluate the statistical significance of each linear regression.

Both CH₄ and O₂ concentrations must be limiting (i.e., close to their respective half-saturation constants) for second-order kinetic control. Methane is likely limiting in all of our samples because it ranges from 0.27 to 19 nmol L⁻¹ and the CH₄ half-saturation constants reported for marine methanotrophs are ≥60 nmol L⁻¹ [Ward and Kilpatrick, 1990]. In contrast, O₂ is likely not a limiting factor in the majority of our samples, because only samples from the core of the OMZ (Figures 2 and 3) approach the 1 μmol L⁻¹ O₂ half-saturation constant [Devol, 1978]. Further, our samples originate from a number of different locations and depths in the ETNP region, which likely host methanotroph communities that vary in number, activity, and kinetic properties. Thus, systematic experimentation with the same methanotroph community (i.e., from the same location and depth) is needed to further examine the possibility of second-order kinetic control.

Generally, longer ³H and LL ¹⁴C turnover times (*t*, the reciprocal of *k*, equation (2)) occur at colder water temperatures, lower CH₄ concentrations, and higher salinities and densities, while faster turnover times are found at warmer temperatures, higher CH₄, and lower salinities and densities (Figure 9a–9h). This relationship with CH₄ has been reported with previous ³H rate measurements [Valentine *et al.*, 2001; Mau *et al.*, 2012] and may indicate the existence of less active methanotroph communities at lower CH₄ levels. The trend with temperature, which is an important factor in all metabolic processes [Gillooly *et al.*, 2001], shows the expected Arrhenius pattern of turnover times increasing as temperatures drop. MO_x rates were not used to investigate environmental correlations because rate calculations incorporate in situ CH₄ concentrations (equation (1)) and thus mathematically correlate MO_x rates with CH₄ concentration.

4.3. Regional MO_x Within the ETNP OMZ

Depth-integrated MO_x rates can provide regional estimates of CH₄ oxidation. In order to examine CH₄ consumption within the OMZ, where the ETNP's large CH₄ pool resides, MO_x rates were depth integrated from 200 to 760 m and multiplied by the ETNP area (5.2 × 10⁶ km²) [Sansone *et al.*, 2001]. These calculations yield regional sink estimates of 4.5–6.1 × 10¹⁰ and 26–100 × 10¹⁰ g CH₄ yr⁻¹ for the LL ¹⁴C and ³H methods, respectively, and show that

substantial methanotrophic activity in the OMZ consumes CH₄ at depth, thereby preventing its eventual release to the atmosphere. MO_x in the OMZ over the ETNP area consumes more CH₄ than that reported for the Eel River Basin (2 × 10⁶ g CH₄ yr⁻¹) [Valentine *et al.*, 2001] and the Juan de Fuca Ridge hydrothermal plume (1.3 × 10⁹ g CH₄ yr⁻¹) [de Angelis *et al.*, 1993], regions that are actively venting CH₄, but cover much smaller areas (25 km² and 170 km², respectively). These data show that slower MO_x rates can indeed integrate to a significant CH₄ sink if functioning throughout a large water volume.

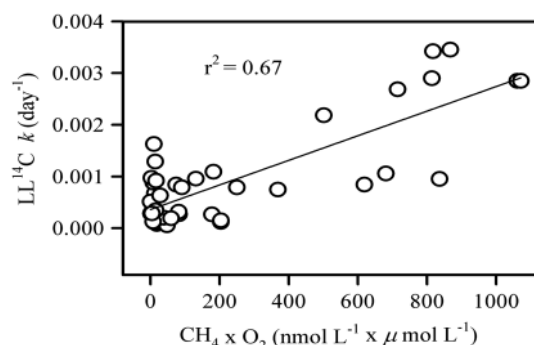


Figure 8. Plot of LL ¹⁴C fractional turnover rates (*k*) versus the product of methane and oxygen concentrations (CH₄ × O₂).

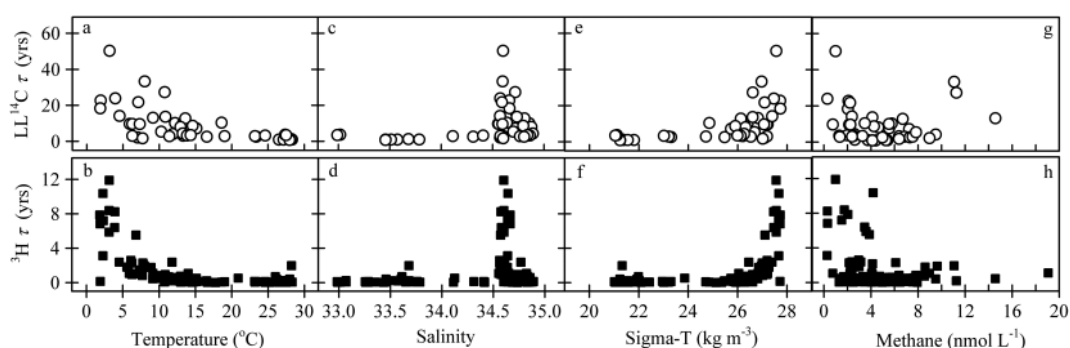


Figure 9. Plots of LL ^{14}C and ^3H turnover times (τ) versus (a, b) temperature, (c, d) salinity, (e, f) density, and (g, h) methane.

Methane in the deeper section of the OMZ (400–760 m) is thought to have advected from organic-rich coastal sediments to the open ocean. Depth-integrated MO_x rates scaled to the ETNP area show that $0.39\text{--}0.44 \times 10^{11} \text{ g CH}_4 \text{ yr}^{-1}$ (LL ^{14}C) or $0.56\text{--}2.6 \times 10^{11} \text{ g CH}_4 \text{ yr}^{-1}$ (^3H) are consumed in this interval of the OMZ. We expect that the amount of CH_4 contributed from coastal sediments to this depth interval is similar to the amount of CH_4 consumed within the interval. This assumes that CH_4 concentrations are not changing with time and that the rate of CH_4 transport out of the OMZ is small compared to MO_x rates.

We scaled up two coastal margin flux measurements to estimate the amount of CH_4 diffusing from coastal sediments (0.24 and $1.7 \mu\text{mol m}^{-2} \text{ d}^{-1}$, open margin sites with water depths in the 400–760 m range from *Sansone et al.* [2004]). Data from Google Earth were used to estimate that a $\sim 17,800 \text{ km}^2$ area of coastal sediment could potentially supply CH_4 to the 400–760 m OMZ waters through diffusion (see Text S2 and Figure S1 in the supporting information). Combining the diffusive fluxes and sediment area yields a source estimate of $0.25\text{--}1.8 \times 10^8 \text{ g CH}_4 \text{ yr}^{-1}$, which is 10^3 smaller than the MO_x sink estimate for the 400–760 m interval. Such a discrepancy suggests the presence of other unidentified CH_4 sources in the region (e.g., areas of greater diffusive flux or ebullition, decomposing methane hydrates) and provides an upper constraint for such sources. Even though the 10^3 difference is large and therefore indicates other sources, the data used for the source and sink estimates is sparse compared to the whole area of the ETNP; thus, we cannot rule out the possibility that the difference is within the error of our calculation.

4.4. MO_x in ETNP Surface Waters

The subsurface CH_4 maximum contributes 25% of the ocean's estimated CH_4 source to the atmosphere [Reeburgh, 2007]. The maximum is thought to be comprised of CH_4 produced locally by methanogens in anaerobic microenvironments or by the biological decomposition of methylphosphonates [Reeburgh, 2007]. MO_x may play a role in mitigating the eventual release of this CH_4 to the atmosphere (e.g., *Nihous and Masutani* [2006]), but previous studies have suggested that sea-air flux is the main sink for CH_4 in open ocean surface waters and that MO_x is not significant [Jones, 1991; Holmes et al., 2000]. Our depth-integrated MO_x rates ($\sim 0\text{--}200$ m, through the subsurface maximum) show that $0.25\text{--}1.3$ and $17\text{--}47 \mu\text{mol CH}_4 \text{ m}^{-2} \text{ d}^{-1}$, for the LL ^{14}C and ^3H methods, respectively, are consumed in ETNP surface waters (Table 4). Whereas, sea-air fluxes of CH_4 from surface waters, estimated using the techniques outlined in *Holmes et al.* [2000], ranged from -0.64 to $9.4 \mu\text{mol CH}_4 \text{ m}^{-2} \text{ d}^{-1}$ (Table 4). The negative flux values at Stations 5 and 6 indicate a CH_4 flux into surface waters, reflecting efficient MO_x that consumes upward fluxes of CH_4 before they reach the atmosphere, as well as some amount of atmospheric CH_4 . At stations with a positive sea-air flux, summing the integrated MO_x rates and sea-air flux values gives an estimate of total CH_4 losses in ETNP surface waters and shows that MO_x on average makes up 25% (LL ^{14}C) or 85% (^3H) of these losses. The results, from both the LL ^{14}C and ^3H methods, show that methanotrophy is a significant sink for CH_4 in ETNP surface waters and that it mitigates the release of CH_4 from the subsurface maximum to the atmosphere.

5. Conclusions

The first MO_x rates reported for the ETNP (1) support the idea that the high CH_4 concentrations in the OMZ come from coastal sediments and persist due to low MO_x rates and (2) show that water column MO_x rates,

Table 4. ETNP Surface Layer Depth-Integrated MO_x Rates, Sea-Air Flux Estimates, and Fraction of ETNP CH_4 Surface Losses Made Up by MO_x^a

| Station | Depth Range ^b (m) | Ing. MO_x Rates | | Sea-Air Flux ($\mu\text{mol CH}_4 \text{ d}^{-1} \text{ m}^2$) | MO_x Fraction ^d | |
|---------|------------------------------|---|--------------|---|-------------------------------------|--------------|
| | | LL ^{14}C ($\mu\text{mol CH}_4 \text{ d}^{-1} \text{ m}^2$) | ^3H | | LL ^{14}C | ^3H |
| | | | | | % | |
| 1 | 6–201 | 1.2 | 17 | 2.1 | 36.2 | 89.2 |
| 2 | 4–199 | na | 47 | 9.4 | na | 83.4 |
| 3 | 4–201 | 1.2 | 24 | 5.5 | 17.7 | 81.5 |
| 4a | 10–242 | na | 25 | 3 | na | 89.2 |
| 5 | 5–170 | na | 40 | −0.16 | ^c | ^c |
| 6 | 4–190 | 0.25 | 19 | −0.64 | ^c | ^c |
| 7 | 5–200 | na | 20 | 5 | na | 80.1 |
| 8 | 5–233 | 1.3 | 38 | 5.6 | 18.5 | 87.2 |

^aThe sea-air fluxes were calculated using the methods outlined in *Holmes et al.* [2000] and an average December 2008 wind speed of 5.8 m s^{-1} from the National Data Buoy Center (<http://www.ndbc.noaa.gov/>, buoy numbers 43301 and 32315).

^bThe depth range used for integration.

^cThe stations with a negative flux indicate a sea-air CH_4 flux into the surface waters and efficient MO_x that comprises all mixed layer losses.

^d MO_x fraction = $100 \times \text{Ing. MO}_x \text{ rates} / (\text{Ing. MO}_x \text{ rates} + \text{Sea-air flux})$.

although slow, still provide a significant internal CH_4 sink that limits the flux of CH_4 from ocean to atmosphere. Future improvements in rate measurement methods, especially if they confirm the ability to measure very low rates with the LL ^{14}C tracer, will further improve our understanding of the role of MO_x in CH_4 ocean-atmosphere fluxes and how they may change in the future when OMZ's are expected to expand.

Several improvements to both the ^3H and LL ^{14}C methods can be recommended for future MO_x rate measurements. The ^3H method background can be better quantified using killed control samples as method blanks (either to subtract from rate samples or set a detection limit [e.g., *Mendes et al.*, 2015]). For this, it is important to treat the killed controls in such a manner that the microbial activity is arrested well before the tracer is added. For the LL ^{14}C method, filters with a pore size of $0.2 \mu\text{m}$ should be used for capturing the bacterial biomass. For both methods, if a Q_{10} correction is to be applied to compensate for incubation temperatures, the sample temperatures need to be limited to a narrow range and be continuously monitored over the incubation to minimize the error associated with a Q_{10} correction. These easily implement updates that should improve ^3H and LL ^{14}C parallel rate measurements; however, highly controlled parallel ^3H and LL ^{14}C rate experiments are required to identify the underlying cause(s) of any remaining discrepancies in parallel rates. Overall, more work is needed to bring all three tracer-based rate measurements (^3H , HL ^{14}C , and LL ^{14}C) in line, and accomplishing this is essential for establishing accurate CH_4 budgets in the ocean water column.

Acknowledgments

The data used throughout this manuscript are available in Table S1 of the supporting information. We thank the officers and crew of the R/V *Knorr* for their support at sea; the Chief Scientist, Kendra Daly, for providing ship time; Kevin Druffel-Rodriguez for his support in the field; John Southon, Sheila Griffin, Aubrey Stills, and Eric Salamanca for their assistance in the laboratory; and John Pohlman and one anonymous reviewer for their very helpful comments; Discussions with John Kessler and Marc Alperin also improved the paper. The National Science Foundation (NSF)-Division of Ocean Sciences (OCE) and the Department of Energy (DOE) provided funding for this work (NSF grant OCE-0622759 to William S. Reeburgh; DOE award DE-NT0005667 to David L. Valentine; DOE fellowship DE-NT0005667 to Monica B. Heintz; and NSF grant OCE-0526545 to Kendra L. Daly).

References

- Burke, R. A., D. F. Reid, J. M. Brooks, and D. M. Lavoie (1983), Upper water column methane geochemistry in the eastern tropical North Pacific, *Limnol. Oceanogr.*, *28*, 19–32, doi:10.4319/lo.1983.28.1.0019.
- Ciais, P., et al. (2013), Carbon and other biogeochemical cycles, in *Climate Change 2013: The Physical Science Basis. Contribution of Working Group I to the Fifth Assessment Report of the Intergovernmental Panel on Climate Change*, edited by T. F. Stocker et al., pp. 465–570, Cambridge Univ. Press, U. K., and New York.
- Cicerone, R. J., and R. S. Oremland (1988), Biogeochemical aspects of atmospheric methane, *Global Biogeochem. Cycles*, *2*, 299–327, doi:10.1029/GB002i004p00299.
- Coleman, D., J. Risatti, and M. Schoel (1981), Fractionation of carbon and hydrogen isotopes by methane oxidizing bacteria, *Geochim. Cosmochim. Acta*, *45*, 1033–1037, doi:10.1016/0016-7037(81)90129-0.
- de Angelis, M. A., M. D. Lilley, E. J. Olson, and J. A. Baross (1993), Methane oxidation in deep sea hydrothermal plumes of the Endeavour Segment of the Juan de Fuca Ridge, *Deep Sea Res., Part I*, *40*, 1169–1186, doi:10.1016/0967-0637(93)90132-m.
- Denman, K. L., et al. (2007), Couplings between changes in the climate system and biogeochemistry, in *Climate Change 2007: The Physical Science Basis. Contribution of Working Group I to the Fourth Assessment Report of the Intergovernmental Panel on Climate Change*, edited by S. Solomon et al., pp. 500–587, Cambridge Univ. Press, U. K., and New York.
- Devol, A. H. (1978), Bacterial oxygen uptake kinetics as related to biological processes in oxygen deficient zones of the oceans, *Deep Sea Res.*, *25*, 137–146.
- Dickens, G. R. (2003), Rethinking the global carbon cycle with a large, dynamic and microbially mediated gas hydrate capacitor, *Earth Planet. Sci. Lett.*, *213*, 169–183.
- Gillooly, J. F., J. H. Brown, G. B. West, V. M. Savage, and E. L. Charnov (2001), Effects of size and temperature on metabolic rate, *Science*, *293*, 2248–2251, doi:10.1126/science.1061967.

- Griffiths, R. P., B. A. Caldwell, J. D. Cline, W. A. Broich, and R. J. Morita (1982), Field observations of methane concentrations and oxidation rates in the Southeastern Bering Sea, *Appl. Environ. Microbiol.*, **44**, 435–446.
- Heeschen, K. U., R. S. Keir, G. Rehder, O. Klatt, and E. Suess (2004), Methane dynamics in the Weddell Sea determined via stable isotope ratios and CFC-11, *Global Biogeochem. Cycles*, **18**, GB2012, doi:10.1029/2003GB002151.
- Heintz, M. B. (2011), Rates of aerobic methane oxidation in the waters of the Santa Monica Basin and Alaskan Arctic Lakes measured with a tritium-based radiotracer technique, PhD thesis, Dep. of Earth Sci., Univ. of Calif., Santa Barbara.
- Heintz, M. B., S. Mau, and D. L. Valentine (2012), Physical control on methanotrophic potential in waters of the Santa Monica Basin, Southern California, *Limnol. Oceanogr.*, **57**, 420–432, doi:10.4319/lo.2012.57.2.0420.
- Hinrichs, K.-U., and A. Boetius (2002), The anaerobic oxidation of methane: New insights in microbial ecology and biogeochemistry, in *Ocean Margin Systems*, edited by G. Wefer et al., pp. 457–477, Springer, Berlin, doi:10.1007/978-3-662-05127-6_28.
- Holmes, M. E., F. J. Sansone, T. M. Rust, and B. N. Popp (2000), Methane production, consumption, and air-sea exchange in the open ocean: An evaluation based on carbon isotopic ratios, *Global Biogeochem. Cycles*, **14**, 1–10, doi:10.1029/1999GB001209.
- Houweling, S., F. Dentener, and J. Lelieveld (2000), Simulation of preindustrial atmospheric methane to constrain the global source of natural wetlands, *J. Geophys. Res.*, **105**, 17,243–17,255, doi:10.1029/2000JD900193.
- Jones, R. D. (1991), Carbon monoxide and methane distribution and consumption in the photic zone of the Sargasso Sea, *Deep Sea Res., Part I*, **38**, 625–635, doi:10.1016/0198-0149(91)90002-w.
- Karl, D. M. (1999), A sea of change: Biogeochemical variability in the North Pacific subtropical gyre, *Ecosystems*, **2**, 181–214.
- Karl, D. M., and B. D. Tilbrook (1994), Production and transport of methane in oceanic particulate organic matter, *Nature*, **368**, 732–734, doi:10.1038/368732a0.
- Karl, D. M., L. Beversdorf, K. M. Björkman, M. J. Church, A. Martinez, and E. F. DeLong (2008), Aerobic production of methane in the sea, *Nat. Geosci.*, **1**, 473–478, doi:10.1038/ngeo234.
- Keir, R. S., J. Greinert, M. Rhein, G. Petrick, J. Sültenfuß, and K. Fühaupter (2005), Methane and methane carbon isotope ratios in the Northeast Atlantic including the Mid-Atlantic Ridge (50°N), *Deep Sea Res., Part I*, **52**(6), 1043–1070, doi:10.1016/j.dsr.2004.12.006.
- Lamontagne, R. A., J. W. Swinnerton, V. J. Linnenbom, and W. D. Smith (1973), Methane concentrations in various marine environments, *J. Geophys. Res.*, **78**, 5317–5324, doi:10.1029/JC078i024p05317.
- Mau, S., M. B. Heintz, and D. L. Valentine (2012), Quantification of CH₄ loss and transport in dissolved plumes of the Santa Barbara Channel, California, *Cont. Shelf Res.*, **32**, 110–120, doi:10.1016/j.csr.2011.10.016.
- Mau, S., J. Blees, E. Helmke, H. Niemann, and E. Damm (2013), Vertical distribution of methane oxidation and methanotrophic response to elevated methane concentrations in stratified waters of the Arctic fjord Storfjorden (Svalbard, Norway), *Biogeosciences*, **10**(10), 6267–6278, doi:10.5194/bg-10-6267-2013.
- Mendes, S. D., M. C. Redmond, K. Voiggritter, C. Perez, R. Scarlett, and D. L. Valentine (2015), Marine microbes rapidly adapt to consume ethane, propane, and butane within the dissolved hydrocarbon plume of a natural seep, *J. Geophys. Res. Oceans*, **120**, 1937–1953, doi:10.1002/2014JC0.10362.
- Naqvi, S. W. A., H. W. Bange, L. Farias, P. M. S. Monteiro, M. I. Scranton, and J. Zhang (2010), Marine hypoxia/anoxia as a source of CH₄ and N₂O, *Biogeosciences*, **7**(7), 2159–2190, doi:10.5194/bg-7-2159-2010.
- Nihous, G. C., and S. M. Masutani (2006), A model of methane concentration profiles in the open ocean, *J. Mar. Res.*, **64**, 629–650, doi:10.1357/002224006778715748.
- Pack, M. A., M. B. Heintz, W. S. Reeburgh, S. E. Trumbore, D. L. Valentine, X. Xu, and E. R. M. Druffel (2011), A method for measuring methane oxidation rates using low-levels of ¹⁴C-labeled methane and accelerator mass spectrometry, *Limnol. Oceanogr. Methods*, **9**, 245–260, doi:10.4319/lom.2011.9.245.
- Pennington, J. T., K. L. Mahoney, V. S. Kuwahara, D. D. Kolber, R. Calienes, and F. P. Chaver (2006), Primary production in the eastern tropical Pacific: A review, *Prog. Oceanogr.*, **69**, 285–317, doi:10.1016/j.pocean.2006.03.012.
- Reeburgh, W. S. (2007), Oceanic methane biogeochemistry, *Chem. Rev.*, **107**, 486–513, doi:10.1021/cr050362v.
- Reeburgh, W. S., B. B. Ward, S. C. Whalen, K. A. Sandbeck, K. A. Kilpatrick, and L. J. Kerkhof (1991), Black-sea methane geochemistry, *Deep Sea Res., Part A*, **38**, S1189–S1210, doi:10.1016/S0198-0149(10)80030-5.
- Rehder, G., R. S. Keir, E. Suess, and M. Rhein (1999), Methane in the northern Atlantic controlled by microbial oxidation and atmospheric history, *Geophys. Res. Lett.*, **26**(5), 587–590, doi:10.1029/1999GL900049.
- Sansone, F. J., B. N. Popp, A. Gasc, A. W. Graham, and T. M. Rust (2001), Highly elevated methane in the eastern tropical north Pacific and associated isotopically enriched fluxes to the atmosphere, *Geophys. Res. Lett.*, **28**, 4567–4570, doi:10.1029/2001GL013460.
- Sansone, F. J., A. W. Graham, and W. M. Berelson (2004), Methane along the western Mexican margin, *Limnol. Oceanogr.*, **49**, 2242–2255, doi:10.4319/lo.2004.49.6.2242.
- Schlitzer, R. (2010), Ocean data view. [Available at <http://odv.awi.de/>]
- Scranton, M. I., and P. G. Brewer (1978), Consumption of dissolved methane in the deep ocean, *Limnol. Oceanogr.*, **23**(6), 1207–1213, doi:10.4319/lo.1978.23.6.1207.
- Valentine, D. L., D. C. Blanton, W. S. Reeburgh, and M. Kastner (2001), Water column methane oxidation adjacent to an area of active hydrate dissociation, Eel River Basin, *Geochim. Cosmochim. Acta*, **65**, 2633–2640, doi:10.1016/S0016-7037(01)00625-1.
- Ward, B. B., and K. A. Kilpatrick (1990), Relationship between substrate concentration and oxidation of ammonium and methane in a stratified water column, *Cont. Shelf Res.*, **10**, 1193–1208, doi:10.1016/0278-4343(90)90016-F.
- Ward, B. B., K. A. Kilpatrick, P. C. Novelli, and M. I. Scranton (1987), Methane oxidation and methane fluxes in the ocean surface-layer and deep anoxic waters, *Nature*, **327**, 226–229, doi:10.1038/327226a0.
- Ward, B. B., K. A. Kilpatrick, A. E. Wopat, E. C. Minnich, and M. E. Lidstrom (1989), Methane oxidation in Saanich Inlet during summer stratification, *Cont. Shelf Res.*, **9**, 65–75, doi:10.1016/0278-4343(89)90083-6.
- Wuebbles, D. J., and K. Hayhoe (2002), Atmospheric methane and global change, *Earth Sci. Rev.*, **57**, 177–210, doi:10.1016/S0012-8252(01)00062-9.
- Xu, X., S. E. Trumbore, S. H. Zheng, J. R. Southon, K. E. McDuffee, M. Luttgen, and J. C. Liu (2007), Modifying a sealed tube zinc reduction method for preparation of AMS graphite targets: Reducing background and attaining high precision, *Nucl. Instrum. Methods Phys. Res., Sect. B*, **259**, 320–329, doi:10.1016/j.nimb.2007.01.175.
- Yamamoto, S., J. B. Alcauskas, and T. E. Crozier (1976), Solubility of methane in distilled water and seawater, *J. Chem. Eng. Data*, **21**, 78–80, doi:10.1021/je60068a029.
- Zhang, X., K. C. Hester, W. Ussler, P. M. Walz, E. T. Peltzer, and P. G. Brewer (2011), In situ Raman-based measurements of high dissolved methane concentrations in hydrate-rich ocean sediments, *Geophys. Res. Lett.*, **38**, L08605, doi:10.1029/2011GL04714.